Journal of Ceramic Processing Research. Vol. 24, No. 1, pp. 134~141 (2023)
(Received 2 July 2022, Received in revised form 24 August 2022, Accepted 26 September 2022)
https://doi.org/10.36410/jcpr.2023.24.1.134

J O U R N A L O F
Ceramic Processing Research

Preparation of layered B_4C with high neutron-shielding properties using graphene as template

Li Yang, Li Sanxi*, Wang Song and Tian Chengcheng
School of Environmental and Chemical Engineering, Shenyang University of Technology, Liaoning 110870, China

In this paper, layered boron carbide (B_4C) particles were successfully synthesized by sol-gel-low temperature pyrolysis method using boron acid and glycerin as raw materials with self-made reduced graphene oxide (RGO) as additives. The structure of the sol-gel condensation product was analyzed by FT-IR. The phase, morphology and particle size of the B_4C were characterized by XRD, FE-SEM and LPSA. The results showed that boron carbide was rhombic crystal phase, but the surface of the particles was wrinkled and more layered. The B_4C powders with uniform morphology and some particle sizes less than 100 nm were prepared with the RGO content of 0.6%. Testing the neutron-shielding properties of the polypropylene-B_4C composites suggested that neutron transmittance with the B_4C content of 35 wt% was 94.1% lower (from 70.6% to 4.1%) than neat polypropylene, and the total macroscopic absorption cross-section was about 18 times larger (from 0.0857 ± 0.0031 cm^{-1} to 1.5521 ± 0.0008 cm^{-1}). The relative density, fracture toughness and hardness of self-made B_4C ceramics (sB_4C) were higher than the commercially available B_4C ceramics (cB_4C). This study provided a new method for the preparation of B_4C powders with excellent neutron absorption properties and good sintering activity.

Keywords: Boron carbide, Graphene, Neutron shielding, Sintering activity.

Introduction

Boron carbide (B_4C) is an important non-metal oxide ceramic with attractive properties of low density, high hardness and high chemical stability, which can be used as cutting tools, abrasives and sandblasting [1-3]. In addition, it is also used as neutron absorber and control rod in nuclear reactors due to its high neutron absorption cross section for the isotope boron (^{10}B) [4-6].

The carbothermic reduction process is the most common commercial method for producing B_4C powder. This process is suitable for quantitative synthesis of boron carbide owing to the raw materials are cheap and harmless [7, 8]. However, this process also has some disadvantages, such as boron loss caused by B_2O_3 volatilization and grain coarsening caused by overtop synthesis temperature [9-11]. Therefore, researchers are more interested in controlling the boron carbide molding process at the molecular level. This process for preparing boron carbide can be roughly divided into three stages: (i) organic sol-gel reaction, (ii) pyrolysis precursor reaction, (iii) carbothermal reduction reaction [12-14]. This technology can effectively reduce the synthesis temperature of boron carbide, and can also solve the problem of grain coarsening during the formation of boron carbide. These researchers used boric acid as the boron source and organic compounds as the carbon source (such as cellulose and glucose [15, 16], citric acid [17-19], glycerin [20-22], phenolic resins [23] and polyethylene alcohols [24-26], etc.) to prepare gels with borate esters (B-O-C). Boron and carbon sources can be dispersed more evenly by sol-gel process, so that the boron carbide powder can be successfully synthesized at a temperature below 1500 °C. The sufficient formation of B-O-C can be induced by adjusting the stoichiometric ratio of boronic acid hydroxyl groups and polyol hydroxyl groups. By adjusting the gas flow, temperature and time during the pyrolysis process, the stoichiometric ratio of boron oxide to amorphous carbon can be controlled. In recent years, porous carbon is often used as carbon source in the preparation of boron carbide to solve the problem of agglomeration of nanoparticles. Porous carbon has also been used as a carbon template owing to its large specific surface area, excellent stability and great shape retention ability. For example, Asgarian et al. [27] and Farzaneh et al. [28] prepared porous and mesoporous carbons using porous and mesoporous materials (sucrose and furfuryl alcohol, respectively) as templates. Then nano B_4C was prepared by magnesium thermal reduction method. However, the process of preparing porous carbon or mesoporous carbon is extremely complex. In addition, the magnesium thermal reduction process assisted by magnesium powder will produce by-products (magnesium oxide and magnesium borate), which will reduce the yield of B_4C [29]. It is very important to choose a suitable production process for the production of boron carbide. Some researchers use a combination of carbonaceous

*Corresponding author:
Tel : +86 18704009103
E-mail: lisx@sut.edu.cn

substances as carbon source for the production of boron carbide. Rafi et al. [35] used citric acid-boron acid to prepare boron carbide, and the addition of ethylene glycol effectively reduced the carbon residue. Moreover, with the increase of ethylene glycol, the morphology of boron carbide changed into needle-like and leaf-like structure. Chen et al. [36] prepared boron carbide by introducing glycerin as additive in the system of polyvinyl alcohol-boron acid. The study found that glycerin can promote the condensation reaction. The distribution of B_2O_3 in carbon network matrix is more uniform, and the free carbon content in boron carbide is greatly reduced. In addition, the morphology of B_4C powder was closely related to the amount of glycerin added. Tahara et al. [37] studied that different molar ratios of tartaric acid were added to glycerin-boron acid system, and then boron carbide powder was prepared by pyrolysis precursor. The dispersion state of the boron oxide and carbon components in the precursor prepared from the condensed product with 25 mol% tartaric acid added was finer than that without tartaric acid added, in which both precursors had a three-dimensional bicontinuous B_2O_3/carbon network structure. The synthesized B_4C powder becomes finer due to the increase of crystal nucleus positions.

Boron (B) element also has a high thermal neutron capture cross section and a wide capture energy spectrum. After absorbing neutrons, only soft γ rays and easily absorbed α particles are generated. It is a better neutron absorbing material. However, pure boron is rarely existed in nature and difficult to manufacture. Most of it exists in the form of boron carbide B_4C. The ^{10}B of B_4C has good neutron absorption performance. B_4C has low cost, no radioactive isotopes, low secondary ray energy, corrosion resistance and good thermal stability. So far, the research on the neutron shielding properties of boron carbide has been a hot topic. Zhang et al. [38] prepared B_4C/Al composites by uniformly dispersing boron carbide in aluminum alloy 6061 by low temperature vacuum hot pressing method. The test results show that the neutron shielding rate of the composite material can reach about 65%. Dai et al. [39] synthesized B_4C/Al composites by powder metallurgy using B_4C and aluminum powder as raw materials. The effect of B_4C mass fraction on the neutron absorption properties of B_4C/Al composites was investigated. The experimental results show that the neutron absorption performance of the composites increases with the raise of boron carbide content. Zali et al. [40] added boron carbide as a filler to polymer to obtain neutron absorption composites with good thermodynamic properties. Harrison et al. [41] carefully studied the effect of filler/polyethylene matrix interfacial interaction on the comprehensive properties of boron nitride/polyethylene composites. Using high-density polyethylene and boron nitride micro-particles (average particle size 7-10 μm) as raw materials, the composite material sheet is made by melt mixing and hot compression molding. Under high-energy neutron irradiation, no long-lived radioactive secondary particles are produced. Irim et al. [42] used boron nitride particles with an average particle size of less than 100 nm and Gd_2O_3 particles to co-fill high-density polyethylene to form a new ternary nanocomposite. Studies have shown that the neutron shielding efficiency of the obtained composites can be increased by 1.5 to 2 times compared with the pure polyethylene samples when the filling fractions of nano-boron nitride and Gd_2O_3 are 5 wt% and 1 wt% to 3 wt%, respectively.

In this study, we found that graphene has a fine wrinkle morphology and porous structure, which can be used as carbon template. It was added to a boron acid-glycerin sol-gel to prepare layered boron carbide by low-temperature pyrolysis precursor method. Compared with Farzaneh's and Liu's research [30], the method used in this study is simpler and the product obtained is purer. In addition, we also explored the influence of the amount of graphene on the particle size and morphology of boron carbide. Finally, the neutron shielding properties of boron carbide polypropylene composites and the mechanical properties of boron carbide ceramics were tested.

Experiment

Materials

Boric acid (99.9%), Bor mining company of Russia; glycerin (analytically pure); concentrated sulfuric acid (analytical grade), Sinopharm Chemical Reagent Co., Ltd; graphite powder (500 mesh), Qingdao Xinghe Graphite Co., Ltd; Potassium permanganate (99.5%), phosphorus pentoxide (98%), potassium persulfate (analytical grade), Guangdong Wengjiang Chemical Reagent; 30% hydrogen peroxide (analytical grade), Changle Xin Fuqiang Co., Ltd.; Concentrated hydrochloric acid (analytical grade), Changzhou Yuanjie Environmental Protection Technology Co., Ltd; Polypropylene, Sinopec Co., Ltd.

Preparation of RGO

In this paper, graphene was prepared by an improved Hummer-chemical reduction method. Graphite powder (5 g), $K_2S_2O_8$ (10 g), P_2O_5 (5 g) and concentrated H_2SO_4 (60 ml) were mixed in a beaker. The temperature was increased to 70 °C as the mixture was stirred for 5 h. After that, filter and wash until neutral, and dry to obtain filter residue. Then slowly add $KMnO_4$ (20 g) into the mixture of filter residue and an appropriate amount of concentrated H_2SO_4 in ice bath with keeping 35 °C for 3 h. Remove excess $KMnO_4$ with H_2O_2 and acidify with 30% HCl. After that, graphene oxide was obtained by water washing, centrifugation and freeze-drying. In a three-necked flask, an appropriate amount of graphene oxide was mixed with 200 ml of ultrapure water and sonicated for 3 h. Then adding hydrazine hydrate and refluxing with heat treatment at 95 °C for 4

h. Graphene (RGO) was obtained by centrifugal washing and drying.

Preparation of B_4C powder

Equimolar glycerin and boric acid were mixed in a 250 ml beaker, and then a certain amount of RGO was added (the amount of RGO was 0%, 0.2%, 0.6% and 1% of the mass of boron acid). Stirring and heating in an oil bath for 150 ℃ until glassy wiredrawing. The product was the RGO condensate. The RGO condensate was heated continuously in 100 ml/min nitrogen flow at a heating rate of 10 ℃/min in three stages. The first stage was heated to 110 ℃ for 1 h. In the second stage, it was heated to 160 ℃ for 1 h. In the third stage, it was heated to 500 ℃ for 3 h. The product was ground to obtain pyrolysis product powders. The pyrolytic product powder was pressed into a black disc with a diameter of 2 cm and a thickness of 0.5 cm. The black disc was heated to 1300-1500 ℃ in 100 ml/min argon flow for 1-5 h. The product boron carbide powder was obtained after cooling.

Preparation of neutron shielding composites

Polypropylene and boron carbide were extruded in a twin-screw extruder. It was placed on a flat hot press with a 10 cm × 10 cm × 5 mm mold, that after pelletizing in the cutter. The neutron shielding composite was obtained after hot pressing and cooling. Neutron shielding composites with B_4C content of 0 wt%, 5 wt%, 10 wt%, 15 wt%, 20 wt%, 25 wt%, 30 wt% and 35 wt% were prepared respectively.

Preparation of B_4C ceramics

Self-hand B_4C powder (6 g) and ultrapure water (2 ml) as coupling agent added into an agate mortar. After manual grinding for 30 min, put the ground slurry into 80 ºC constant temperature drying oven for drying. The dried powder was sieved through 30 meshes. The screened powder was filled into the graphite mold, putting in vacuum hot-pressing furnace to sintered in 30 MPa with hot treatment at 2000 ºC for 2 h. B_4C ceramics (sB_4C) can be obtained after cooling. In the same way, the commercially available B_4C powder was made into B_4C ceramics (cB_4C) as the control group.

Characterization

The structure of the condensation product was characterized by prestige-21 Fourier transform infrared spectrometer (FT-IR); Xrd-7000 X-ray diffractometer (XRD) was used to determine the phase of the product; SU8010 field emission scanning electron microscope (FE-SEM) was used to observe the morphology and distribution of the crystal. Bt-90 nano laser particle size analyzer (LPSA) of Dandong Baite Instrument Co., Ltd. was used to determine the particle size of the product. According to Archimedes' principle, the bulk density of B_4C ceramics was measured with distilled water as the medium. When calculating the relative density of B_4C ceramics, 2.52 g/cm^3 was selected as the theoretical density of B_4C. After the prepared B_4C ceramics were polished, the fracture toughness and hardness of the ceramic sheets are tested by nano indentation. The data of ten points were measured for each sample, and then the average value was taken.

Results and Discussion

RGO Characterization

Fig. 1 and Table 1 showed the EDS analysis diagram of RGO. There are mainly three elements of C, N, and O in RGO (as shown in Fig. 1), and the carbon content in RGO was 89.78% (as shown in Table 1). In the subsequent preparation of B_4C powder, the molar ratio of carbon to boron was calculated according to the carbon content in RGO. As Fig. 2 showed, the micro morphology of RGO. It can be seen from Fig. 2a that the size of RGO was about 4-5 μm. Two-dimensional lamellar structure of the RGO was expressed in Fig. 2c, which proved that it had excellent toughness and ductility. Fig. 2b showed that there are many wrinkles on the surface of the sheet, which may be caused by the stacking of graphene sheets [31].

Table 1. Elemental analysis results of RGO.

Sample	C (wt%)	N (wt%)	O (wt%)
RGO	89.78	5.89	4.32

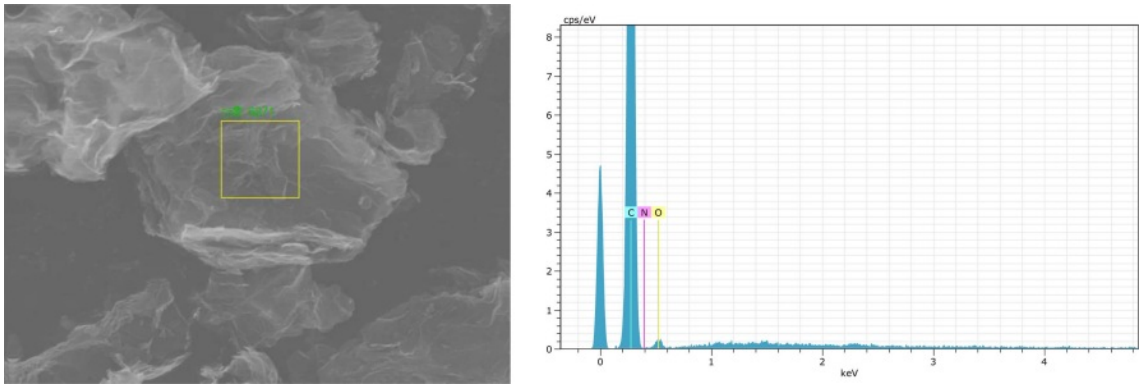

Fig. 1. EDS analysis of reduced graphene oxide.

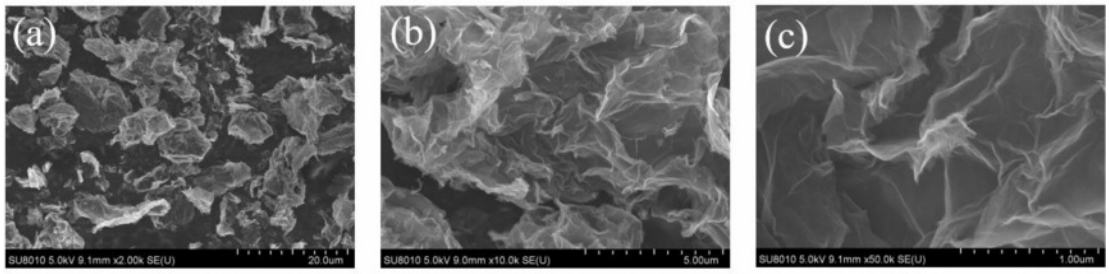

Fig. 2. FE-SEM images of RGO (a) 2000 times, (b) 10000 times, (c) 50000 times.

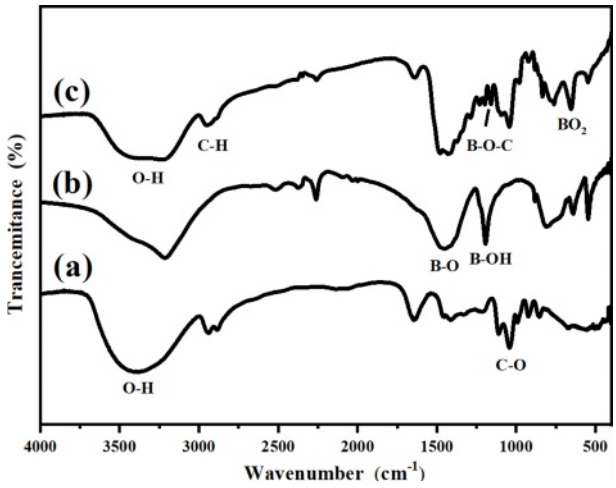

Fig. 3. FT-IR spectra of (a) glycerin, (b) boron acid and (c) 0.6% RGO condensate.

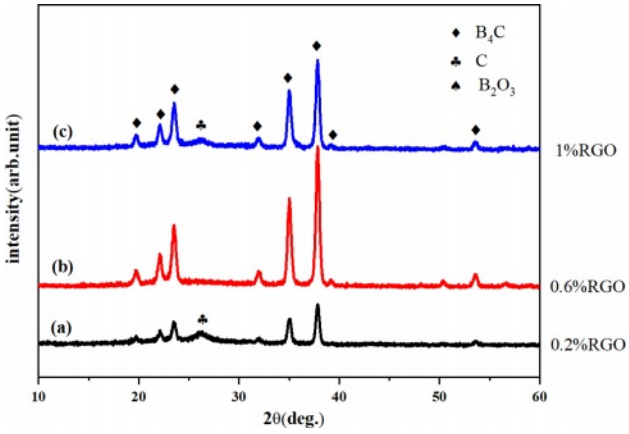

Fig. 4. XRD pattern of B_4C powder with the addition amount of RGO (a) 0.2%, (b) 0.6% and (c) 1%, the carbothermic reduction temperature is 1450 °C and the reaction time is 3 h.

Structural analysis of RGO condensate

The bonding state of the RGO condensate was characterized using FT-IR. The FT-IR spectrum in Fig. 3 performed glycerin, boron acid and 0.6% RGO condensate. The absorption peak at 1035 cm^{-1} for glycerin (Fig. 3a) was the C-O stretching vibration mode and that at 1500 cm^{-1} for H_3BO_3 (Fig. 3b) was assigned to the B-O stretching vibration mode [14], these peaks were also observed for the condensed product (Fig. 3c). Note that O-H stretching bands are clearly observed at approximately 3300 cm^{-1} for the raw materials, H_3BO_3 and glycerin (Fig. 3a and Fig. 3b), whereas they are relatively weaker for the condensed product (Fig. 3c). The bending vibration peak of B-O-C was observed at 1159 cm^{-1}, it means that B-O-C bonds were formed in the prepared condensed product across the whole sample. Compared with the study by Kakiage et al. [21], the addition of graphene did not change the condensation state of boron acid and glycerin.

Phase analysis of B_4C powder

As shown in Fig. 4, the XRD results indicated that B_4C formed rhombohedral phase (JCPDS-ICCD #35–0798). The addition of RGO was 0.2% and 1% (Fig.4a and Fig. 4c) emerged wide peak at 2θ=26.6°, which was caused by carbon residue. This was attributed to the fact that the ratio of boron oxide and amorphous carbon was not controlled within a reasonable range during the pyrolysis process, resulting in carbon residues in the subsequent carbothermic reduction reaction. The content of H_3BO_3 was determined by titration, and the change in the C/B_2O_3 ratio was calculated as shown in Fig. 5. The condensation products of RGO with different additions amount were

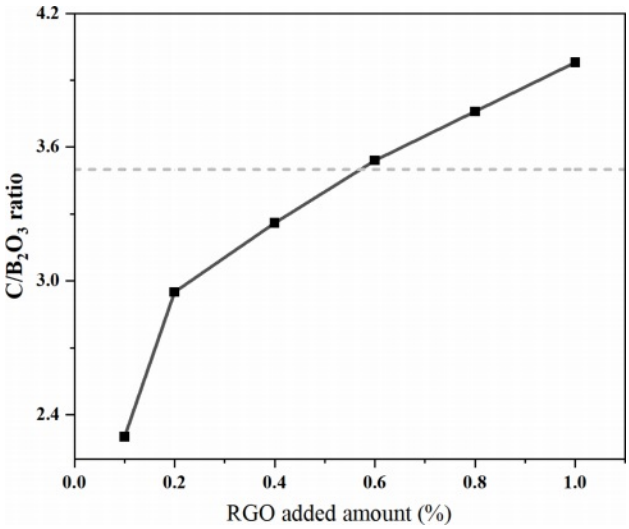

Fig. 5. Changes in the C/B_2O_3 ratio of the precursor powder prepared by pyrolysis at 500 °C for 2 h for condensation products with graphene additions of 0% to 1%. The dotted line indicates that the stoichiometric ratio C/B_2O_3 is 3.5.

pyrolyzed at 500 °C for 2 h to prepare precursor powder, and the B_2O_3 component was recovered after washing with hot water. It can be seen that when the addition amount of RGO was 0.6%, the C/B_2O_3 ratio in the pyrolysis product was closest to 3.5. Therefore, the pyrolysis precursor of 0.6% RGO as the raw material for carbothermal reduction, relatively pure B_4C powder can be obtained. The peak intensity ratio of B_4C was estimated according to the XRD pattern of each product to evaluate the formation behavior of B_4C [32-34, 43]. The change of B_4C formation behavior was caused by the difference in the uniformity and dispersion of B_2O_3 and carbon components in the precursor. It can be seen that in the experimental group with 0.6% RGO added, the peak intensity ratio is the largest. This is due to the appropriate addition amount, which makes the diffusion of the reactants easier, and the boron-carbon components are more uniformly dispersed, so relatively pure products are obtained.

Morphology analysis of B_4C powder

Fig. 6 showed the microstructure analysis of B_4C powder with RGO addition of (a) 0% (b) 0.2%, (c) 0.6% and (d) 1%, carbothermal reduction temperature of 1450 °C and reaction time of 3 h. There are many wrinkles and honeycomb shape on B_4C particles (as shown in Fig. 6b). The possible reason was that RGO as template induces B_4C of rhombic phase, which makes the surface protrusions of B_4C increase. However, the particle size of B_4C was not uniform due to the existence of some large particles in the self-made RGO. With the increasing of the content of RGO, the irregular folds are gradually reduced, and a single particle tends to grow into a rod (from Fig. 6b to Fig. 6d). This may be due to the increase of the content of RGO, which makes the stacking of the lamellar structure more closely. Fig. 7 showed the particle size analysis spectrum of B_4C powder with RGO addition amount of (a) 0.2%, (b) 0.6% and (c) 1%, carbothermal

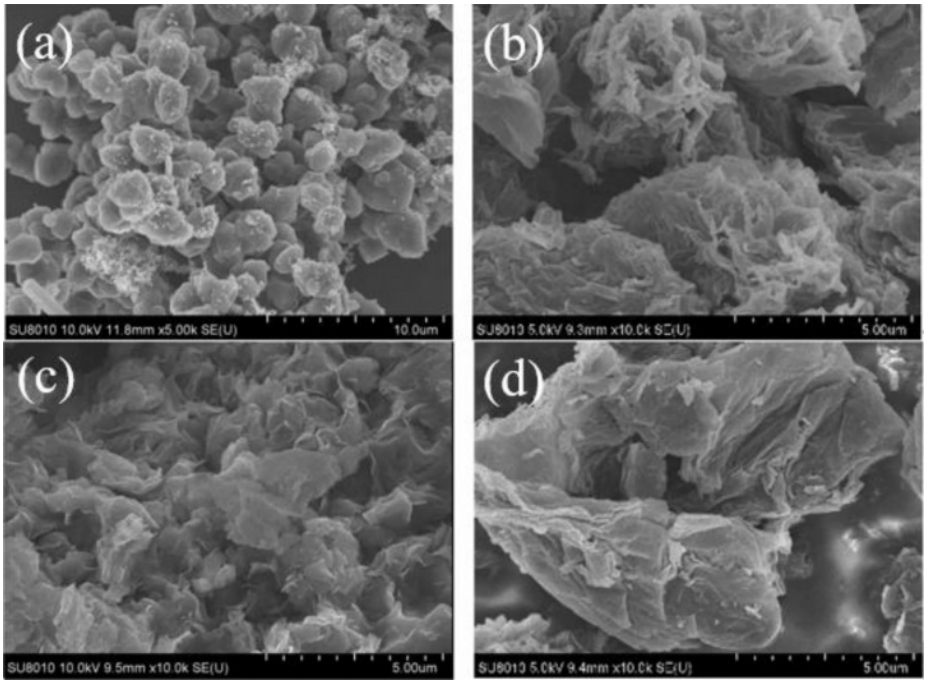

Fig. 6. FE-SEM micrographs of B_4C powder with the addition amount of RGO (a) 0%, (b) 0.2%, (c) 0.6% and (d) 1%, the carbothermic reduction temperature is 1450 °C and the reaction time is 3 h.

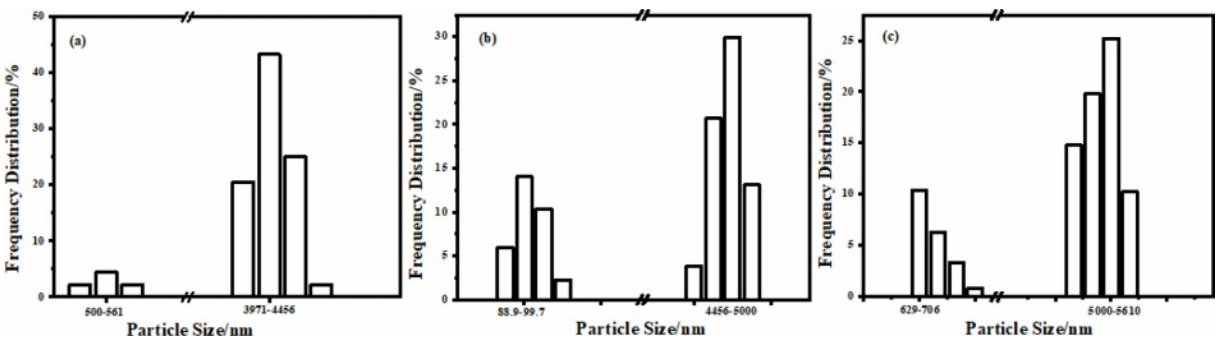

Fig. 7. The particle size analysis spectrum of B_4C powder with the addition amount of RGO (a) 0.2%, (b) 0.6% and (c) 1%, the carbothermic reduction temperature is 1450 °C and the reaction time is 3 h.

reduction temperature of 1450 ℃ and reaction time of 3 h. When the amount of RGO added was 0.2%, 0.6% and 1%, the corresponding median diameters were about 4.2 um, 4.6 um and 5.4 um, respectively (as shown in Fig. 7a, Fig. 7b and Fig. 7c). The particle size of B_4C powder was positively correlated with the amount of RGO added, which was basically consistent with that shown in Fig. 6. Some B_4C particles are smaller than 100 nm in Fig. 7b, which may be attributed to the more uniform mixing and dispersion of boron oxide and carbon during low-temperature pyrolysis. In addition, by observing the particle size distribution in Fig. 7, as the addition amount increases of RGO, the particle size distribution becomes narrower and narrower. This was attributed to the increase of RGO content, which makes the B_2O_3 and carbon components have a larger contact area, resulting in the formation of more nucleation sites and a more uniform particle size distribution.

Neutron shielding performance

The B_4C powder prepared with 0.6% RGO was melt-blended with polypropylene to prepare the composite material. The effect of B_4C content on the neutron transmittance of neutron shielding composites as shown Fig. 8. The B_4C contents of the composites were 0 wt%, 5 wt%, 10 wt%, 15 wt%, 20 wt%, 25 wt%, 30 wt% and 35 wt%, respectively. All samples were 5 mm thickness. The neutron transmittance of composite decreases significantly which the content of B_4C was 5%. Its dependence of neutron transmittance on B_4C content gradually decreases with the further increase of B_4C content, but the curve still performed downward trend. The neutron transmittance of the composite (B_4C, 35 wt%) reaches the lowest (only 4.1%). The neutron transmittance of the composites decreased from 70.6% (B_4C, 0 wt%) to 4.1% (B_4C, 35 wt%), indicating that the transmittance of the composites with 35 wt % B_4C

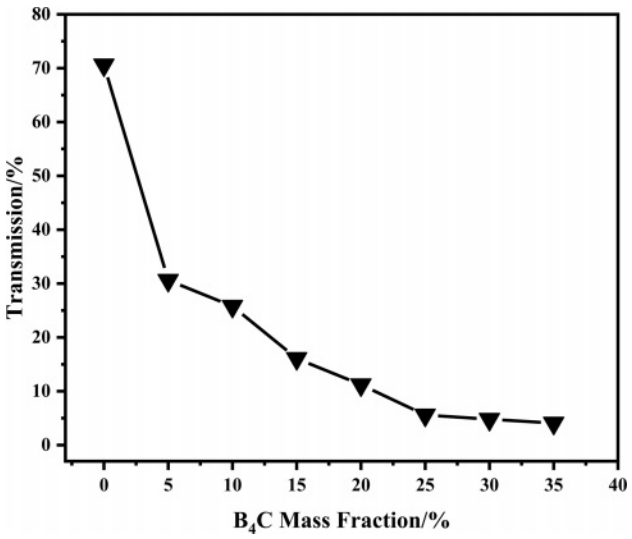

Fig. 8. Neutron transmittance of neutron-shielding composites with different B_4C contents.

Table 2. Total absorption macroscopic cross-section as a function of B_4C content in Neutron shielding composites.

B_4C content (%)	Total absorption macroscopic cross-section Σ (cm^{-1})
0	0.0857 ± 0.0031
5	0.5452 ± 0.0018
10	0.7562 ± 0.0012
15	0.9365 ± 0.0012
20	1.0536 ± 0.0012
25	1.2536 ± 0.0008
30	1.5331 ± 0.0008
35	1.5521 ± 0.0008

decreased by 94.1% compared to the composites without B_4C. The ability of a neutron shielding material to capture neutrons can be expressed in Eq. (1):

$$I/I_o = e^{-\Sigma\chi} \quad (1)$$

Where I and Io are the intensity of the incoming neutron and the transmitted neutron respectively; ∑ is the total macroscopic absorption cross section; χ represents the thickness of composite.

Table 2 summarizes the total macroscopic absorption cross-sections of the prepared neutron shielding composites. The total macroscopic absorption cross section of neat polypropylene is 0.0857 ± 0.0031 cm^{-1}. The total macroscopic absorption cross-section of the neutron shielding composites increases with the increase of B_4C content due to the high neutron absorption properties of boron element. For the composite with 35 wt% B_4C content, the total macroscopic absorption cross section increased by about 18 times (from 0.0857 ± 0.0031 cm^{-1} to 1.5521 ± 0.0008 cm^{-1}). The composites filled with B_4C showed a higher total macroscopic absorption cross-section for thermal neutrons, which may be due to the tendency of layered boron carbide to be superimposed in the longitudinal direction of the material when it was added to the polypropylene matrix. It can capture neutrons more efficiently when colliding with neutrons. The larger surface area of B_4C particles in the wrinkled shape promotes a higher probability of neutron interaction, which effectively improves the neutron shielding performance of the composite material.

Mechanical property test

In order to prove that the synthesized B_4C powder had excellent sintering activity which can effectively improve the sintering compactness and fracture toughness of B_4C ceramics. The SEM images were compared of the commercially available B_4C powder (Fig. 9) and the self-made B_4C (Fig. 6c) that the particle size of B_4C was basically identical, but the morphology had great differences. The commercially available products were regular diamond shaped particles. The

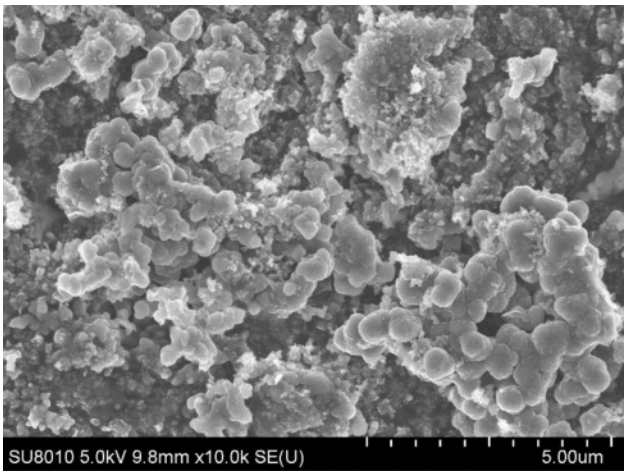

Fig. 9. SEM images of commercially available B_4C powders.

Table 3. Comparison of relative density, fracture toughness and hardness of two ceramics prepared.

Sintering Temperatures (°C)	Samples	Relative Density (%)	Racture Toughness (MPa/m^2)	Hardness (GPa)
2000	sB_4C	98.36	4.26	19.33
	cB_4C	93.54	3.12	17.12

results of testing mechanical properties were expressed in Table 3 both cB_4C and sB_4C. The relative density of sB_4C (98.36%) was higher than that of cB_4C (93.54%), which it was probably related to the layered structure on the surface of the self-made B_4C powder. This layered structure had large specific surface area, many internal defects and large lattice distortion, which it was beneficial to increase the sintering driving force and improve the sintering compactness of ceramics. The hardness of sB_4C and cB_4C were 19.33 Gpa and 17.12 Gpa, respectively. It may be that the high sintered density of the ceramics reduces the number of pores in the ceramics as crack sources, thereby increasing the hardness of the ceramics. The better fracture toughness of the sB_4C (4.26 MPa/m^2) may be due to the fact that the B_4C powder used for sintering contains RGO, and the graphene with high specific surface area can cross each other to form a lubricant network to resist the applied stress.

Conclusion

In this paper, B_4C powder with layered structure was successfully prepared by low temperature pyrolysis precursor method. FT-IR results showed that the addition of RGO did not affect the structure of the boron acid-glycerin condensation products. The RGO prepared in the laboratory had obvious lamellar structure. The morphology of B_4C powder was greatly affected by the templating of RGO, which its particles showed layered wrinkle shape. The B_4C powders with uniform morphology and some particle sizes less than 100 nm were prepared with the RGO content of 0.6%. The neutron shielding performance test results indicated that the neutron transmittance decreases with the increase of B_4C content in composite. Compared with the neat material, the neutron transmittance of the composite with 35 wt% B_4C content decreased by 94.12%, and the corresponding total macro cross section increased by about 18 times. The test results of mechanical properties showed that the relative density, fracture toughness and hardness of sB_4C were significantly higher than cB_4C. The self-made B_4C powder had high sintering activity. This study provides a new idea for B_4C to control templated growth from the molecular level in the future. Our group will continue to do research work on B_4C morphology control.

Acknowledgement

The authors would like to acknowledge financial support from Key Laboratory of Liaoning Province for Polymer Catalytic Synthesis, Liaoning Provincial Engineering Laboratory for Advanced Polymeric Materials and High-tech Research and Development Project of Liaoning Provincial Industrial Special Resources Protection Office (Liao Cai Qi [2013] 736).

References

1. C.-A. Sun, X.-G. Lu, Y.-B. Chen, L.-L. Zuo, and Y.-K. Lie, J. Ceram. Process. Res. 22[3] (2021) 340-344.
2. P. Svec, Z. Gabrisova, and A. Brusilova, J. Ceram. Process. Res. 20[1] (2019) 113-120.
3. T. Jiang, H.-Y. Jin, Z.-H. An, J. F. Yang, and G.-J. Qiao, J. Ceram. Process. Res. 10[1] (2009) 113-116.
4. H.-K. Wei, Y.-J. Zhang, and X.-Y. Deng, J. Ceram. Process. Res. 12[5] (2011) 599-601.
5. R. Alexander, T.S.R.C. Murthy, K. Vasanthakumar, N.S. Karthiselva, S.R. Bakshi, and K. Dasgupta, Ceram. Int. 44[17] (2018) 21132-21137.
6. D.-J. Yan, J.-K. Liu, X.-C. Fu, P.-L. Liu, and H.-A. Luo, J. Mater. Sci. 54[8] (2019) 6151-6163.
7. R. Adeli, S.P. Shirmardi, and S.J. Ahmadi, Radiat. Phys. Chem. 127 (2016) 140-146.
8. R.-C. Chen, Q.-Q. Shi, L. Su, M. Yang, Z.-Y. Huang, Y.-L. Shi, Q.-H. Zhang, Z.-J. Liao, and T.-C. Lu, Ceram. Int. 43[1] (2017) 571-577.
9. J. Kenny, N. McDonald, J. Binner, I.T. H. Chang, and S. Marinel, J. Eur. Ceram. Soc. 42[2] (2021) 383-391.
10. P.-H. Li, M.-D. Ma, Y.-J. Wu, X. Zhang, Y.-K. Chang, Z.-W. Zhu-Ge, L. Sun, W.-T. Hu, D.-L. Yu, B. Xu, Z. Zhao, J. Chen, J. He, and Y. Tian, J. Eur. Ceram. Soc. 41[7] (2021) 3929-3936.
11. O. Karaahmet and B. Cicek, Ceram. Int. 48[9] (2022) 11940-11952.
12. S. Avcioglu, F. Kaya, and C. Kaya, Ceram. Int. 47[19] (2021) 26651-26667.
13. D.-H. Ding, B. Bai, G.-Q. Xiao, J.-Y. Luo, and X.-C. Chong, Ceram. Int. 47[13] (2021) 18708-18719.
14. S.K. Vijay, R. Krishnaprabhu, V. Chandramouli, and S.

Anthonysamy, Ceram. Int. 44[5] (2018) 4676-4684.
15. Y.-C. Zheng, Z.-Q. Li, J. Xu, T.-L. Wang, X. Liu, X.-H. Duan, Y.-J. Ma, Y. Zhou, and C.-H. Pei, Nano Energy 20[4] (2016) 94-107.
16. S. Akihiro, K. Hidetaka, H. Hiroki, and K. Hajime, Carbon 226[19] (2007) 8-12.
17. A. Sinha, T. Mahata, and B.P. Sharma. J. Nucl. Mater. 301[2-3] (2002) 165-169.
18. A.K. Khanra, Bull. Mater. Sci. 30[2] (2007) 93-96.
19. A.M. Hadian and J.A. Bigdeloo, J. Mater. Eng. Perform. 17[1] (2008) 44-49.
20. S.K. Vijay, R. Krishnaprabhu, V. Chandramouli, and S. Anthonysamy, Ceram. Int. 44[5] (2018) 4676-4684.
21. M. Kakiage, N. Tahara, I. Yanase, and H. Kobayashi, Mater. Lett. 65[12] (2011) 1839-1841.
22. S.-J. Wang, Y.-F. Li, X.-L. Xing, and X.-L. Jing, J. Mater. Res. 33[11] (2018) 1659-1670.
23. A. Najafi, F. Golestani-Fard, H.R. Rezaie, and N. Ehsani, J. Alloys Compd. 509[37] (2011) 9164-9170.
24. N. Shawgi, S.-X. Li, and S. Wang, Ceram. Int. 43[13] (2017) 10554-10558.
25. N. Shawgi, S.-X. Li, S. Wang, Y. Li, and R. Ramzi, Ceram. Int. 44[1] (2018) 774-778.
26. N. Shawgi, S.-X. Li, S. Wang, Z. Wang, and Y.- N. Nie, J. Solgel Sci. Technol. 82[2] (2017) 450-457.
27. P. Asgarian, A. Nourbakhsh, P. Amin, R. Ebrahimi-Kahrizsangi, and K.J.D. MacKenzie, Ceram. Int. 40[10] (2014) 16399-16408.
28. F. Farzaneh, F. Golestanifard, M.S. Sheikhaleslami, and A.A. Nourbakhsh, Ceram. Int. 41[10] (2015) 13658-13662.
29. E. Karacay, E. Alp, and H.C. Cabbar, J. Fac. Eng. Archit. Gaz. 27[2] (2012) 417-428.
30. Y.-J. Liu, Q. Tian, S.-Q. Wang, Z.-Q. Li, X.-H. Duan, L.-K. Que, and C.-H. Pei, Ceram. Int. 46[11] (2020) 18131-18141.
31. I. Yanase, R. Ogawara, and H. Kobayashi, Mater. Lett. 63[1] (2009) 91-93.
32. N. Shawgi, S.-X. Li, S. Wang, Y. Li, and R. Ramzi, Ceram. Int. 44[8] (2018) 9887-9892.
33. O. Karaahmet and B. Cicek, Ceram. Sili. 64[4] (2020) 434-446.
34. R. Ramzi, S. Wang, N. Shawgi, S.-X. Li, and T. Tang, Mater. Res. Express. 6[3] (2018) 203-210.
35. Rafi-ud-din, G.H. Zahid, Z. Asghar, M. Maqbool, E. Ahmad, T. Azhar, T. Subhani, and M. Shahzad, J. Asian Ceram. Soc. 2[3] (2014) 268-274.
36. X.-W. Chen, S.-M. Dong, Y.-M. Kan, H.-J. Zhou, J.-B. Hu, and Y.-S. Ding, Rsc. Adv. 6[11] (2016) 9338-9343.
37. N. Tahara, M. Kakiage, I. Yanase, and H. Kobayashi, J. Alloys Compd. 573[19] (2013) 58-64.
38. P. Zhang, Y.-L. Li, W.-X. Wang, Z.-P. Gao, and B.-D. Wang, J. Nucl. Mater. 437[1] (2013) 350-358.
39. Z.-L. Dai, X.-Q. Liu, and Z.-L. Liu, Acta. Physuca. Sinca. 14[8] (2014) 36-39.
40. N. Zali, H. Yazid, M.H. Ahmad, I. Abdul-Rahman, and Y. Abdullah, Mater. Sci. Forum 888[25] (2017) 179-183.
41. H. Courtney, W. Sean, B. Craig, B. Eric, H. Nolan, and G. Eric, J. Appl. Polym. Sci. 109[4] (2008) 2529-2538.
42. I.S. Gozde, W.A. Alchekh, K.M. Aker, B. Oktay, O. Guralp, A. Ahmet, D. Mahmut, and K. Msut, Radiat. Phys. Chem. 144 (2017) 434-443.
43. O. Seung-Keun, K.S. Do, K. Youngman, and P.S. Sub, J. Ceram. Process. Res. 17[7] (2016) 763-767.